



## Article

# Similarity Analysis between Contour Lines by Remotely Piloted Aircraft and Topography Using Hausdorff Distance: Application on Contour Planting

Alexandre Araujo Ribeiro Freire <sup>1,\*</sup> , Mauro Antonio Homem Antunes <sup>2</sup> , Murilo Machado de Barros <sup>2</sup> ,  
Wagner Dias de Souza <sup>2</sup> , Wesley de Sousa da Silva <sup>2</sup> and Thaís Machado de Souza <sup>2</sup>

<sup>1</sup> Technical School, Federal Rural University of Rio de Janeiro, Seropédica 23890-000, RJ, Brazil

<sup>2</sup> Engineering Department, Federal Rural University of Rio de Janeiro, Seropédica 23890-000, RJ, Brazil; mauroantunes@ufrj.br (M.A.H.A.); barrosmm@ufrj.br (M.M.d.B.); wagners@ufrj.br (W.D.d.S.); wesleyss@ufrj.br (W.d.S.d.S.); thaaismds@ufrj.br (T.M.d.S.)

\* Correspondence: alexandrefreire@ufrj.br

**Abstract:** Contour planting minimizes soil degradation, making agricultural production more sustainable. Currently, geotechnologies can provide more precise and fast data from relief than rudimentary data acquisition for agricultural management. Thus, the objective of this work was to analyze the similarities between contour lines from topography and Remotely Piloted Aircraft, using the Hausdorff distance algorithm. This study was carried out in the period between January 2020 and November 2021 in four localities in the State of Rio de Janeiro, Brazil: two areas located in the municipality of Bom Jardim and two areas in the municipality of Seropédica. Data were acquired through a conventional topographic survey and an aerial photogrammetric survey by Remotely Piloted Aircraft. From the acquired field data for the studied areas, the Digital Elevation Models were generated with a spatial resolution of 0.20 m and the contour lines with an equidistance of one meter. The contour lines obtained by both techniques were superimposed and their similarity was verified using the Hausdorff distance. The results show that there was a better similarity among the contour lines in areas with a very rugged relief than in a smooth relief. Also, the lowest altimetric differences observed in the Digital Elevation Models were associated with the smallest Hausdorff distance. These adjustments correspond, respectively, to the segments between the contour lines with the best and the worst individual similarity for each area. We observed that the similarity between the contour lines from topography and RPA yielded slope differences lower than 6.1% for at least 95% of all studied areas. The Hausdorff distance analysis allowed us to conclude that contour planting can be performed from data obtained via Remotely Piloted Aircraft, provided that vertical accuracy analysis controls the quality of the Digital Elevation Models.

**Keywords:** aerial photogrammetry by Remotely Piloted Aircraft; contour planting; Digital Elevation Model



**Citation:** Freire, A.A.R.; Antunes, M.A.H.; de Barros, M.M.; de Souza, W.D.; de Sousa da Silva, W.; de Souza, T.M. Similarity Analysis between Contour Lines by Remotely Piloted Aircraft and Topography Using Hausdorff Distance: Application on Contour Planting. *Remote Sens.* **2022**, *14*, 3269. <https://doi.org/10.3390/rs14143269>

**Academic Editors:**  
Diego González-Aguilera, Jose A. Jiménez-Berni, Ittai Herrmann, Shangpeng Sun and Monica Herrero-Huerta

Received: 27 May 2022

Accepted: 4 July 2022

Published: 7 July 2022

**Publisher's Note:** MDPI stays neutral with regard to jurisdictional claims in published maps and institutional affiliations.



**Copyright:** © 2022 by the authors. Licensee MDPI, Basel, Switzerland. This article is an open access article distributed under the terms and conditions of the Creative Commons Attribution (CC BY) license (<https://creativecommons.org/licenses/by/4.0/>).

## 1. Introduction

Food demand is expected to increase, and the rational use of natural resources available on Earth becomes an incontestable premise from any perspective in the near future. Soil is one of the most precious and necessary resources for agricultural activities, and because of it, its use must be subjected to processes that increasingly generate less damage to the environment.

Conservation agricultural practices play a key role in a sustainable agricultural production scenario [1]. Agricultural productivity could expand without an increase in environmental degradation if the amount of impact per unit of product or activity were reduced [2].



Among the usable conservation practices, contour planting is one of the viable options to preserve soil erosion processes, according to Santos et al. [3], Griebeler et al. [4], Leite et al. [5], and Xavier et al. [6]. Contour planting contributes to sustainability by controlling the loss of soil particles so that the soil becomes more resistant to the erosive process [7]. In this context, techniques that result in more efficient agricultural production [8], such as implementing Intelligent Agriculture practices will become relevant for preserving natural resources [9].

Presenting different technologies to farmers will allow them to acquire skills to achieve socially, economically, and environmentally advanced agriculture technology [1]. From this premise, geotechnologies contribute to decision making, providing promising tools to perform different analyzes in rural space which can be used as a means of control and knowledge concerning land use [10,11].

Hunt and Daughtry [12] and Maes and Steppe [13] reviewed the progress of remote sensing with Remotely Piloted Aircrafts (RPAs) in the scope of Precision Agriculture (PA). The authors emphasized that the focus of the most recently discussed applications in the scientific environment has been the detection of water stress, pathogens, and pesticide applications, monitoring and detection of weeds, and assessment of the nutritional status, growth, biomass, and yield forecast of crops. Literature reviews on this subject are available in Bendig et al. [14], Pérez-Ortiz et al. [15], Chang et al. [16], Schut et al. [17], Tsouros, Bibi, and Sarigianni-dis [18], Santos et al. [19] and Delavarpour et al. [20].

RPAs generate digital cartographic products, such as Digital Elevation Models (DEMs) [21,22] and slope maps [23,24], which are necessary for the discretization of the relief, where the farming will be installed. Such products are considered indispensable for several farmland management, e.g., coffee [25]. Coffee is generally growing on sloping lands and contour planting provides a well-distributed crop, increasing operational efficiency, mainly those arising from mechanized activity [25,26].

For digital cartographic products via RPA it is necessary to proceed with the quality data analysis referring to the DEMs and their derived attributes, e.g., the contour lines for the correct application in PA. This work presented a new perspective regarding the use of RPAs in the data acquired, i.e., similarity analysis by the Hausdorff distance algorithm among the contour lines compared to a more accurate elevation data source, such as conventional topography. The objective of this comparison is based on the use of the contour lines from aerial photogrammetry by RPAs, to carry out contour planting, optimizing the PA cycle.

## 2. Study Area

We selected four rural localities in the State of Rio de Janeiro, Brazil: two properties located in the municipality of Bom Jardim, in the Mountain Region of Rio de Janeiro, and two areas located at the Federal Rural University of Rio de Janeiro (UFRRJ), in the lowlands of Rio de Janeiro, municipality of Seropédica.

Areas 1 and 2 are located in the municipality of Bom Jardim. The first area of approximately 0.344 ha, between latitude  $22^{\circ}17'23.987''\text{S}$ – $22^{\circ}17'21.494''\text{S}$ , longitude  $42^{\circ}20'6.930''\text{W}$ – $42^{\circ}20'3.157''\text{W}$ , the slope average of 38.4%. The second area of approximately 0.183 ha, between latitude  $22^{\circ}17'30.056''\text{S}$ – $22^{\circ}17'28.826''\text{S}$ , longitude  $42^{\circ}19'54.851''\text{W}$ – $42^{\circ}19'52.368''\text{W}$ , the average slope 41.2%. Both sites at the time of data acquisition (January 2020) had collard (*Brassica oleracea*, Acephala group), plantations carried out in beds, with an average height of the crop around 0.25 m, planted intermittently, without weeds and the interference of trees or buildings in the polygon of interest. Bare soil was predominant in these two areas.

Areas 3 and 4 are located on the UFRRJ campus. Area 3 of approximately 1044 ha, between latitude  $22^{\circ}47'11.965''\text{S}$ – $22^{\circ}47'6.392''\text{S}$ , longitude  $43^{\circ}40'49.271''\text{W}$ – $43^{\circ}40'44.625''\text{W}$ , and an average slope 6.5%. Area 4 of approximately 0.756 ha, between latitude  $22^{\circ}46'47.015''\text{S}$ – $22^{\circ}46'40.282''\text{S}$ , longitude  $43^{\circ}41'7.111''\text{W}$ – $43^{\circ}41'2.119''\text{W}$  and slope average of 6.3%. Both areas had grass cover at a height close to 0.05 m with patches of bare soil and without the interference



of trees or buildings in the polygon of interest at the time of image acquisition in November 2021.

According to the Brazilian soil classification system [27], areas 1 and 2 have topography characterized as very rugged relief. Areas 3 and 4 have topography characterized as smooth relief. Figures 1 and 2 present the four study areas separated by region and the spatial distribution of the control and checkpoints to perform the external orientation of the images and the quality control.

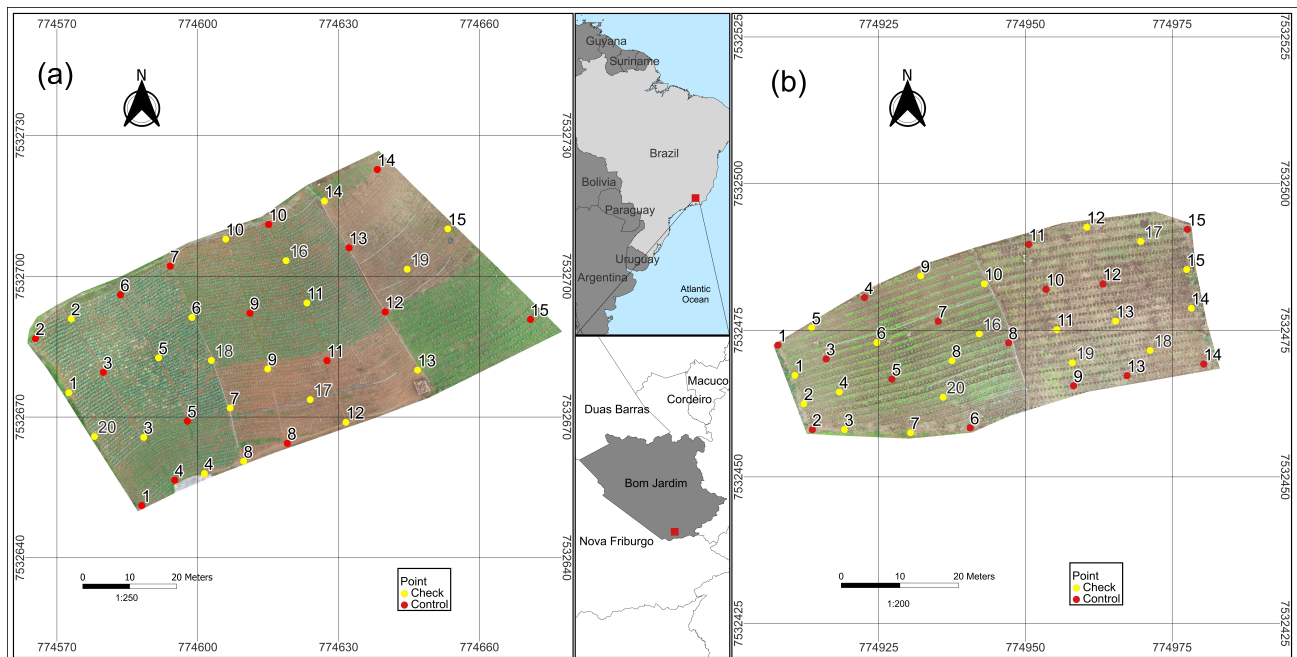


**Figure 1.** Orthophotomosaic of area 1 (a) and area 2 (b), with their respective control and checkpoints.

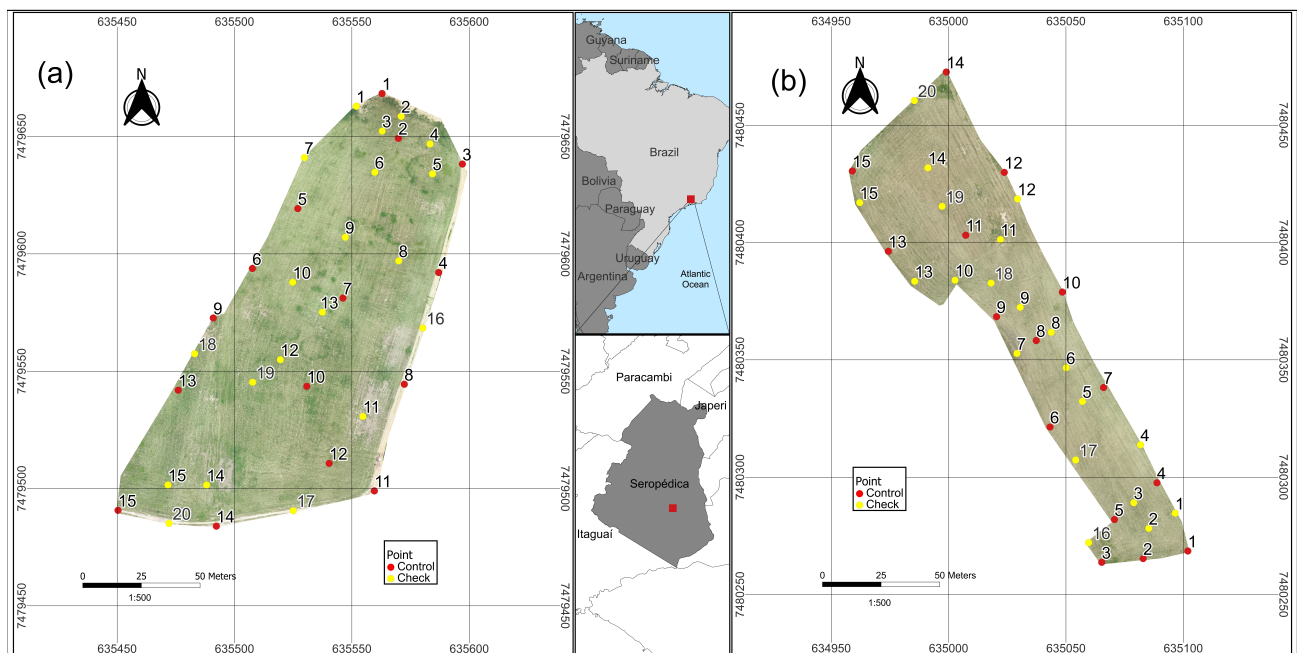


**Figure 2.** Orthophotomosaic of areas 3 (a) and area 4 (b), with their respective control and checkpoints.



### 3. Data and Methods

#### 3.1. Data Acquisition and Analysis

In this section, the procedures for data acquisition and analysis were presented according to the steps shown in the flowchart (Figure 3).

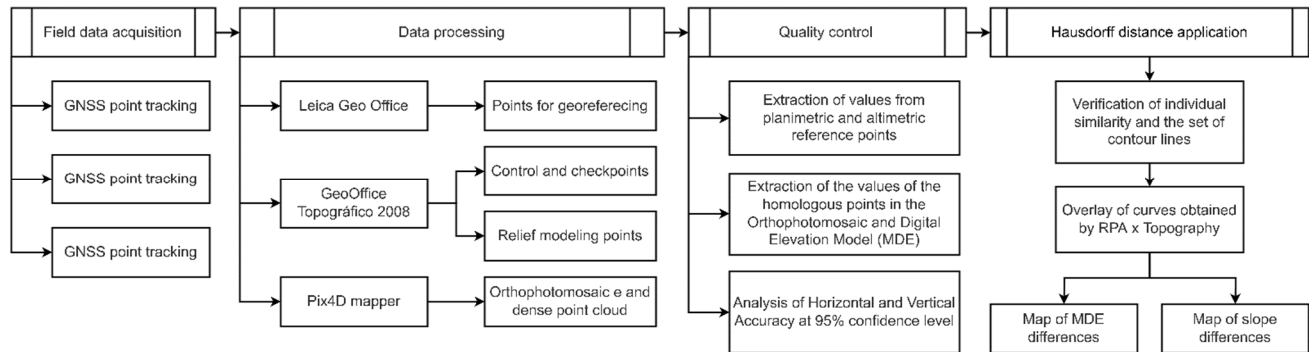


**Figure 3.** Flowchart for data acquisition and analysis.

The following sections presented the detailed steps in Figure 3.

##### 3.1.1. Tracking Points by GNSS

We chose a pair of GNSS points implanted in the field in each of the four studied areas for georeferencing topographical points and to carry out the external orientation of the images obtained by the RPA. The tracking was performed using the fast static relative type method, with three hours of occupancy at each vertex. The equipment used was a dual-frequency (L1, L2) Spectra Precision EPOCH 25 GNSS receiver, performing the data post-processing using the Leica Geo Office software.

The processing was made with the coordinates (E, N, and h) of the control stations originating from the Brazilian Network for Continuous Monitoring of GPS (RBMC), located in the municipalities of Niterói (RJNI) and Vassouras (RJVA), State of Rio de Janeiro, Brazil. The coordinates were extracted from the descriptions of the databases provided by the Brazilian Institute of Geography and Statistics (IBGE), responsible for regulating the Brazilian Geodetic System (SGB). The geoid height component (N) was used to convert the ellipsoidal height (h) into orthometric height (H), where N was calculated from the MAPGEO 2015 software provided by the IBGE.

We defined the reference ellipsoid and the projection system for the elaboration of the products of interest. For this purpose, the elliptical Geodetic Reference System 1980 (GRS80) was used in the Geocentric Reference System for the Americas (SIRGAS 2000). The GRS80 ellipsoid was used due it is the basis of SIRGAS 2000, the current Geodetic Reference System of the SGB. The projection system was the Universal Transverse Mercator (UTM), Zone 23 South, central meridian equal to 45°W.

##### 3.1.2. Conventional Topographic Survey

The topographic planialtimetric survey was carried out using a total station, Spectra Precision, model Focus 2 by the irradiation method. The equipment has a nominal angular precision of 2 s and a nominal linear precision of 2 mm + 2 ppm, classified as a high precision device according to the Brazilian Standard (NBR) 13.133 (Brazilian Association of Technical Standards—ABNT, 1994) which regulates topographic surveys.

The topographic survey aimed to register the relief variations of the areas for the production of DEMs, contour lines, and topographic slope maps, as shown in Figures 4 and 5. We surveyed the 15 control points and 20 checkpoints implemented in the field, as reference for the processes inherent to the aerial photogrammetric survey by RPA and subsequent validation in the quality control stage. The polygonal and topographic irradiation data were processed using the GeoOffice Topographic 2008 software v. 2.8.4.0,



exporting the attributes spreadsheet in text format and the “.txt” extension to ArcGis V. 10.8. In the GIS environment, Digital Elevation Models were generated and then contour lines and slope maps were derived. To perform these operations, the “Topo to Raster” interpolator was used. This interpolation algorithm is based on iterative finite differences to generate a regular grid from elevation points and/or contour lines ESRI [28]. According to Hutchinson [29], the “Topo to Raster” uses known information from surface elevation, such as elevation points (such as in this work), contour lines, and water body delimitations, among others. Also, according to the author, the insertion of this information optimizes the resolution of the DEM, improving the quality of the generated product.

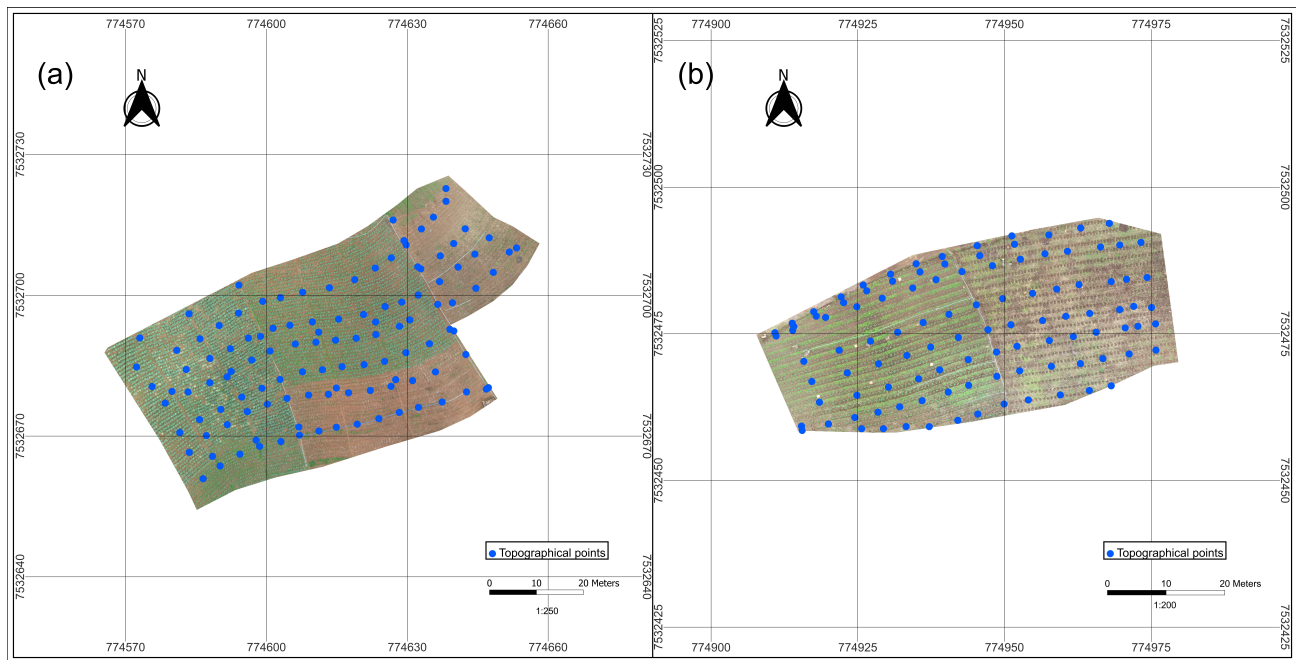


**Figure 4.** Surveyed points from the areas of Bom Jardim municipality: (a) location of points registered in area 1 by conventional topographic survey and (b) location of points registered in area 2 by the conventional topographic survey.

### 3.1.3. Remotely Piloted Aircraft Survey

The RPA Phantom 4 Pro equipment was used to carry out the aerial photogrammetric survey (Figure 6). The 20-megapixel CMOS camera was programmed to obtain aerial images at previously stipulated time intervals and according to the flight plan prepared for the area.

The aerial photogrammetric survey was conducted following the steps: flight planning, field implementation of control points and checkpoints, image acquisition, project configuration, and the digital processing of the images.

Initially, the prior planning was prepared through the Drone Deploy application, with the information relevant to the flight lines configured for the imaging of the areas. Then, we defined the flight height of 60 m, flight direction in the longitudinal direction, and lateral and longitudinal overlaps of 80% and 80%, respectively, for the four areas.

Before the flight, we checked the propellers' fixation, the energy load of the remote control and the aircraft, the amount of satellite signal the RPA was receiving and enabled the starting point system, checked the compass, radio, IMU, and gimbal calibration using DJI GO v.4 software (DJI, G.O.4, 2017).

After the flight, the digital processing of the images was performed using the software Pix4D mapper v. 4.5.6. This software automatically calculated the positions and orientations of the original images obtained using the RPA through aerial triangulation, finally performing the bundle block adjustment. The interior and exterior orientation parameters



were provided and recognized by the software automatically, as they were in the RPA camera library.

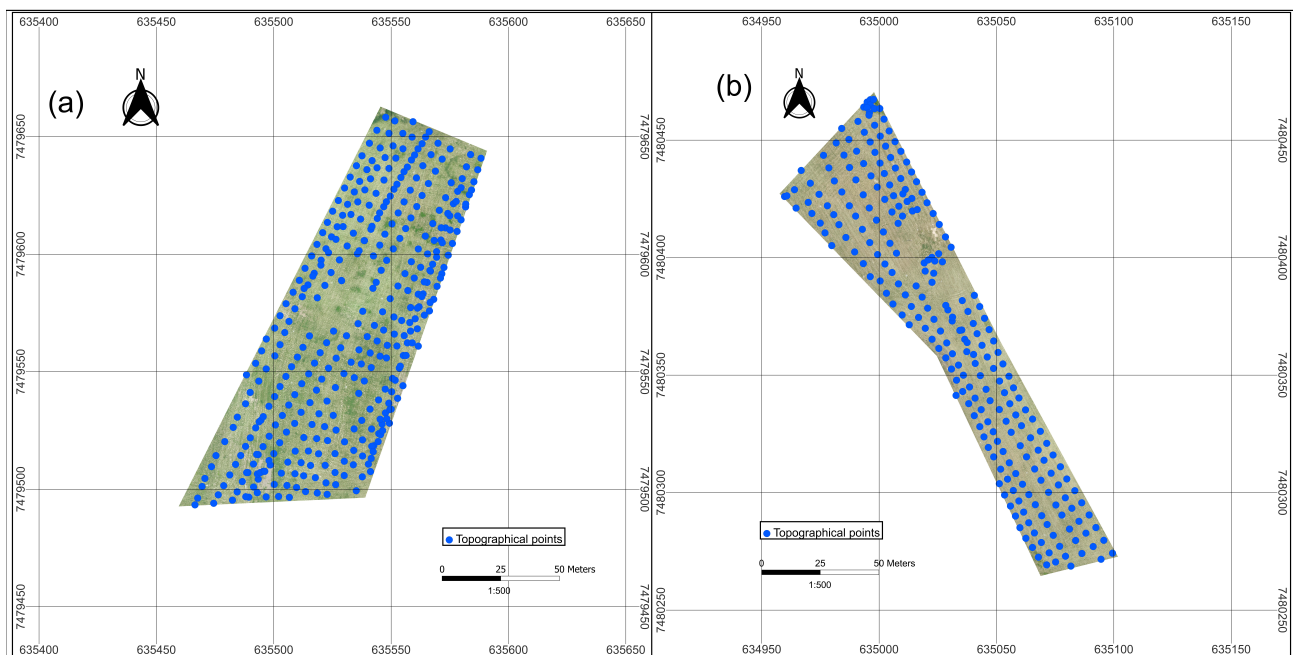


**Figure 5.** Surveyed points from the areas of Seropédica municipality: (a) location of points registered in area 3 by conventional topographic survey and (b) location of points registered in area 4 by the conventional topographic survey.

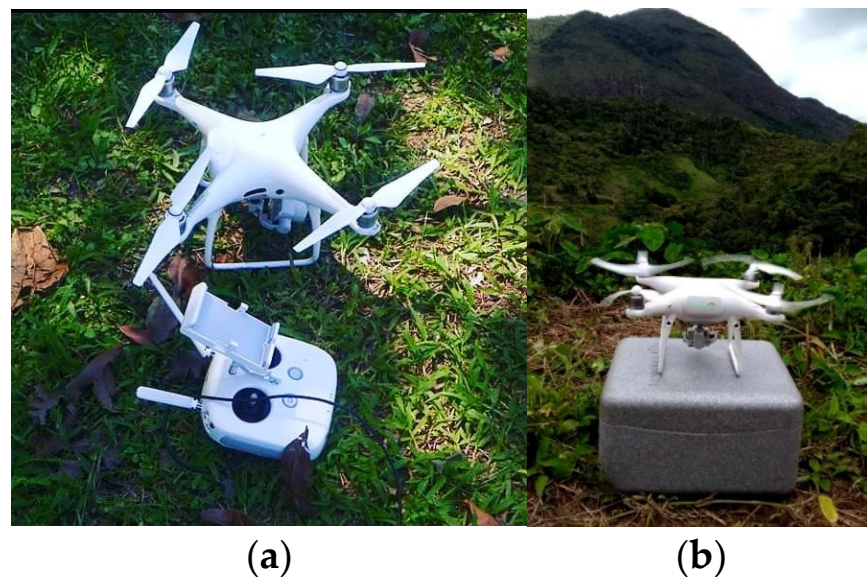


**Figure 6.** Phantom 4 Pro RPA for field survey. (a) Above view, and (b) Side view.

In the Pix4D mapper environment, all three processing steps were performed automatically [30]. These steps followed interior orientation, automatic correspondence among images imported into the software, and with some overlap, the simultaneous bundle block adjustment, and the generation of final products, such as the orthophotomosaic and the dense point cloud generation. However, in the external orientation stage in the image orthorectification process, the control points in the images were identified manually with the insertion of their respective coordinates.

The Structure from Motion (SfM) algorithm, which uses the combined approach to know the pattern of correspondence in the images, was used to derive dense point clouds



in three dimensions (3D) from the images obtained by the camera coupled to RPA [31]. Initial processing was performed by selecting the Pre-Set Standard 3D Maps option, using the original image scale. Digital Surface Models (DSM) were generated, performing the automatic filtering procedure for the dense cloud of points generation. The densification of the point cloud was performed based on the original scale of the image. The density of points of the dense cloud was elaborated with the optimized parameter (Pix4D default).

After performing the steps of digital image processing, orthophotomosaics and dense point clouds were generated for all areas in the Pix4D mapper software, which were exported in LAS format to the ArcGIS software. In the GIS environment, the data were processed to obtain the DEMs, derive the contour lines, and prepare the slope maps, using the “Topo to Raster” interpolator.

In a GIS environment, the coordinates E (m), N (m), and H (m) of homologous points to the checkpoints registered by topography were extracted from the orthophotomosaics and the DEMs of areas 1, 2, 3, and 4. This procedure was necessary to carry out the planimetric and altimetric quality control of the generated digital cartographic products.

### 3.2. Quality Control

The product accuracy measured by comparing its information with those observed in the field is more reliable and of better quality. The verification of the accuracy of the product was determined based on statistical parameters linked to a certain level of confidence adopted, following the standardization recommended for each country [32]. Therefore, those obtained by conventional topography were considered reference data, as one of the most accurate methods for obtaining data [33]. Therefore, the digital cartographic products obtained through RPA were considered data to be validated.

The assessment of the positional accuracy of the orthophotomosaics and the altimetric accuracy of the DEMs was based on the Positional Accuracy Standards for Digital Geospatial Data (PASDGD) (ASPRS 2014), considering open terrain and areas without vegetation (NVA classification) [34]. This was possible because the vegetation had low heights in the four areas (0.25 m in areas 1 and 2 with mostly bare soil and 0.05 m in areas 3 and 4 with patches of bare soil). GeoPEC software v. 3.5.2 was used to evaluate the horizontal and vertical accuracy, where the coordinate data of the 20 checkpoints (reference and test) in each area were inserted through a file (.txt). The ASPRS PASDGD standard was used for the analysis of geospatial datasets based on the Root Mean Square Error (RMSE) statistic of the checkpoints. The RMSE was obtained as a function of the difference between the reference coordinates and the observed coordinates, for the three axes (x, y, and z), as presented in Equations (1)–(3), respectively [35].

$$RMSE_x = \sqrt{\frac{1}{n} \sum_{i=1}^n (X_{reference} - X_{test})^2} \quad (1)$$

where:

n is the number of samples;

$X_{reference}$  as coordinate value (x) in the reference product (m);

$X_{test}$  as coordinate value (x) in the product tested (m).

$$RMSE_y = \sqrt{\frac{1}{n} \sum_{i=1}^n (Y_{reference} - Y_{test})^2} \quad (2)$$

where:

n is the number of samples;

$Y_{reference}$  as coordinate value (y) in the product reference (m);

$Y_{test}$  as coordinate value (y) in the reference product (m).



$$RMSE_z = \sqrt{\frac{1}{n} \sum_{i=1}^n (Z_{reference} - Z_{test})^2} \quad (3)$$

where:

$n$  is the number of samples;

$Z_{reference}$  as coordinate value ( $z$ ) in the reference product (m);

$Z_{test}$  as coordinate value ( $z$ ) in the reference product (m).

From the results found in the RMSE<sub>x</sub> and RMSE<sub>y</sub>, the value of the RMSE<sub>r</sub> (radial direction) was determined using Equation (4) [36].

$$RMSE_r = \sqrt{(RMSE_x^2) + (RMSE_y^2)} \quad (4)$$

After RMSE<sub>r</sub> and RMSE<sub>z</sub> results, horizontal (Equation (5)) and vertical (Equation (6)) accuracy values were calculated for each of the areas, according to the PASDGD standard (ASPRS 2014).

$$Accuracy_r = 1.7308 \times RMSE_r \quad (5)$$

$$Accuracy_v = 1.960 \times RMSE_z \quad (6)$$

### 3.3. Hausdorff Distance Application

The Hausdorff distance (dH) algorithm was used to quantify the similarity between the homologous contour lines referring to the digital products generated by two different data acquisition techniques. According to Gregoire and Bouillot [37], the algorithm had its conception developed by Felix Hausdorff, according to Equation (7):

$$dH(A, B) = \sup\{h(A, B), h(B, A)\} \quad (7)$$

where:

$dH(A, B)$ : as Hausdorff distance.

$\sup$ : as the highest value between two data set.

$h(A, B)$ : as the highest distance between the minimum data set from A to B.

$h(B, A)$ : as the highest distance between the minimum data set from B to A.

$h(A, B)$  and  $h(B, A)$  were given by Equations (8) and (9):

$$h(A, B) = \sup\{\min_{b \in B}\{d\{(a, b)\}\}\} \quad (8)$$

$$h(B, A) = \sup_{b \in B}\{\min_{a \in A}\{d\{(b, a)\}\}\} \quad (9)$$

According to data sets (A and B), which are the linear features that describe the contour lines, the Euclidean distance from each point  $a \in A$  to all points  $b \in B$  was determined. The data set (A) is composed of contour lines from conventional topography (reference line), whereas the data set (B) is formed by contours obtained via RPAs (test line). Figure 7 represents the distance from the data set A to B ( $d1$ ) and the distance from data set B to A ( $d2$ ) between the reference line (LR) and the test line (LT).

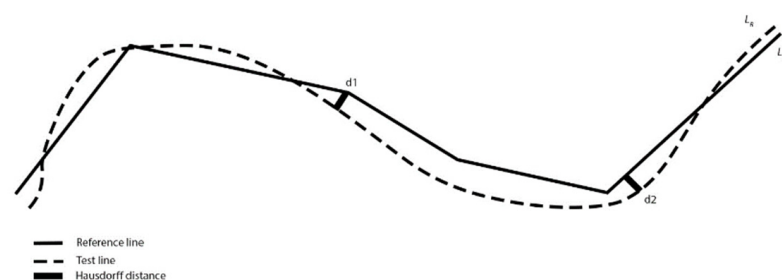


Figure 7. Hausdorff distance survey. Adapted with permission from Santos et al. [38].



The smallest distances between the points in the data set A to B were determined, and the supreme value of the smallest ones was taken, that is, the greatest distance between the smallest measured distances was fixed. This same process was repeated, starting from data set B to A. At the end of the process, two maximum values  $h(A,B)$  and  $h(B,A)$  were determined, therefore, the dH was the biggest value.

The analysis of the dH algorithm between the contour lines was performed with the aid of the similarity checker software, developed for this experiment. For such, the user inserted the data in the format (GeoJSON) of the georeferenced files containing the contour lines of both representations to be compared.

From the insertion of the data, the software applied the algorithm based on the recognition of the elevation of the homologous contour lines and their georeferenced positioning, returning with the dH for each pair of curves. The similarity of a cartographic representation obtained by different techniques can be individually and jointly analyzed, determining statistical parameters such as mean ( $\bar{x}$ ), standard deviation ( $\sigma$ ), maximum (max), and minimum (min) distance from a set of contour lines in the same representation.

Finally, the contour lines were superimposed on the maps that represent the altimetric differences and the resulting slope differences between both techniques to associate them with the results found by the dH.

### 3.4. Database System Application of Hausdorff Algorithm

A Database System (DBS) was created for the application of the Hausdorff algorithm, which is composed of, at least, an application program, a Database Management System (DBMS), and a Database [39]. The flowchart for using this system is shown in Figure 8. The application program for this system was available on a website divided into front-end and back-end. Apache Lounge 2.4 was used on the Windows 10 Pro operating system to provide this application on a local network.

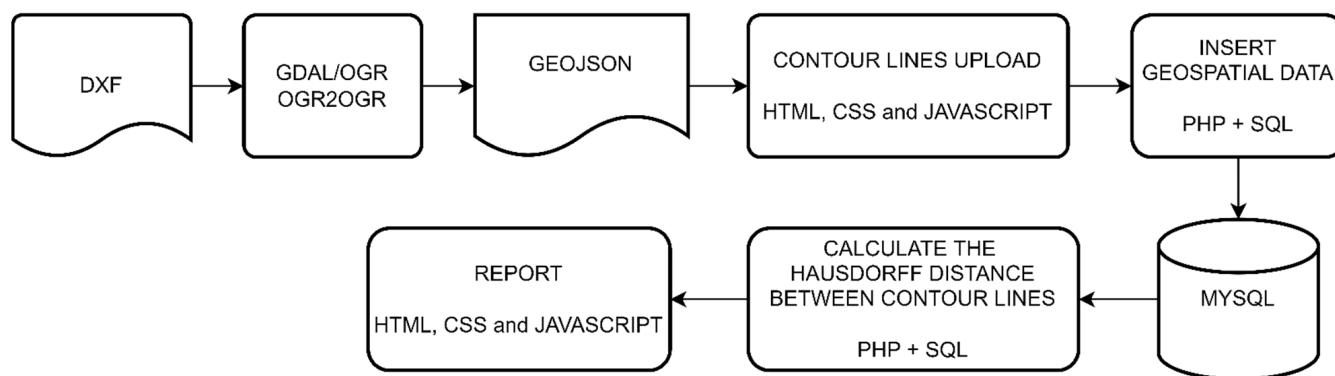


**Figure 8.** Flowchart of the Database System.

The HTML, the CSS style, and the Javascript programming languages were used to develop the front end. The Hypertext Preprocessor (PHP) version 8.1 and Standard Query Language (SQL) were used for the back-end implementation, while the MySQL Community Server DBMS version 8.0 was used for geospatial data storage.

Thus, the application consisted of a Web system with a Geographic Database. MySQL was chosen due to its fast processing speed and spatial function with the implementation of the Hausdorff distance algorithm between two linear features. This function is called “ST\_HausdorffDistance” and can calculate the similarity of two different geometries inserted in the WEB system.

Data entry in this system was performed by uploading a file in GeoJSON format [40,41]. The choice of GeoJSON was based on their fast processing speed, easy data readability by humans and machines, reduced file size, and full compatibility between all software technologies used in this work. Therefore, all contour lines were created or converted to a file in GeoJSON format. The European Petroleum Survey Group (EPSG) Geodetic Parameter



Dataset of the geospatial data used corresponds to the MySQL-controlled geographic database. EPSG 31983 was configured in the SIRGAS 2000 Reference System, zone 23 S, Central Meridian 45°W, of the UTM Projection System.

The “ogr2ogr” is a Geospatial Data Abstraction Library (GDAL/OGR) command-line tool to convert one OGR Simple Features Library into another. In this work procedure, the software “ogr2ogr” was used to convert files in DXF format, which contained the contour lines, to files in GeoJSON format. However, the file in GeoJSON format was constructed with features of the type LineString (shown in the blue rectangle of Figure 9) and each point of the LineString had the three axes x, y, and z.

```

1 {
2   "type": "FeatureCollection",
3   "name": "entities",
4   "crs": { "type": "name", "properties": { "name": "urn:ogc:def:crs:EPSG::31983" } },
5   "features": [
6     {
7       "type": "Feature",
8       "properties": {
9         "Layer": "AREAL_ARP_REC2",
10        "SubClasses": "AcDbEntity:AcDb3dPolyline",
11        "EntityHandle": "69" },
12        "geometry": {
13          "type": "LineString",
14          "coordinates": [ [ 774644.394759248942137, 7532719.995867665857077, 877.0 ], ... ] } },
15    {
16      "type": "Feature",
17      "properties": {
18        "Layer": "AREAL_ARP_REC2",
19        "SubClasses": "AcDbEntity:AcDb3dPolyline",
20        "EntityHandle": "E4" },
21        "geometry": {
22          "type": "LineString",
23          "coordinates": [ [ 774659.094501582672819, 7532707.735314433462918, 871.0 ], ... ] } },
24    ...,
25    ...,
26    ...
27  ]
28 }

```

**Figure 9.** Example of a system input GeoJSON file.

Thus, the z coordinate consisted of the elevation of the contour lines (shown in the red rectangle in Figure 9). The z coordinate value is used in the software to sort and organize the contour lines in this system.

The contour lines were uploaded by the user via the website’s graphical interface. After performing this procedure, the system’s back-end received and sent the geospatial data to be stored in a MySQL database. After correctly populating the geographic database, spatial queries were created using SQL. A new webpage was developed to present the results of these queries. On this webpage, the results obtained according to the dH algorithm between the linear features, which represent the contour lines, were presented in table format. In Figure 10, the PHP and SQL code of the query is analyzed to calculate the Hausdorff distance between curves of different geospatial objects in MySQL. Figure 11 shows the PHP and SQL implementation of the query to calculate the Hausdorff distance between contour lines in a single MySQL geospatial object.



```

$query=""
for($i=1; $i<=$total_curves; ++$i){
    $query .= "
        SELECT
            ROUND(
                ST_HausdorffDistance(
                    ST_GeometryN(ct.curves, $i),
                    ST_GeometryN(cd.curves, $i),
                    'metre'
                ),
                3
            ) as hausdorff_distance
        FROM curves ct, curves cd
        WHERE ct.id < cd.id
        UNION
    ";
}
$query = trim(preg_replace('/\s+/S', " ", $query));
$query = substr($query, 0, -6);
$query .= ";";
$result_query = mysqli_query($connection, $query);

```

**Figure 10.** Implementation of the query in PHP and SQL to obtain the Hausdorff distance among features of different geospatial objects.

```

$query=""
for($i=1; $i<$total_curves; ++$i){
    $query .= "
        SELECT
            ct.id as method_id,
            $i as id_a,
            $i+1 as id_b,
            ROUND(
                ST_HausdorffDistance(
                    ST_GeometryN(ct.curves, $i),
                    ST_GeometryN(ct.curves, $i+1),
                    'metre'
                ),
                3
            ) as hausdorff_distance,
        FROM curves ct, curves cd
        WHERE ct.id = cd.id
        UNION
    ";
}
$query = trim(preg_replace('/\s+/S', " ", $query));
$query = substr($query, 0, -6);
$query .= " ORDER BY id_a;";
$result_query = mysqli_query($connection, $query);

```

**Figure 11.** Implementation of the query in PHP and SQL to obtain the Hausdorff distance among features of the same geospatial object.



## 4. Results and Discussion

### 4.1. Differences in Relief Modeling

The DEMs were generated for areas 1, 2, 3, and 4 from the topographic and aerial photogrammetric surveys. Subsequently, the map algebra operation among their respective products was carried out to obtain the altimetric difference between both techniques (Figures 12 and 13).

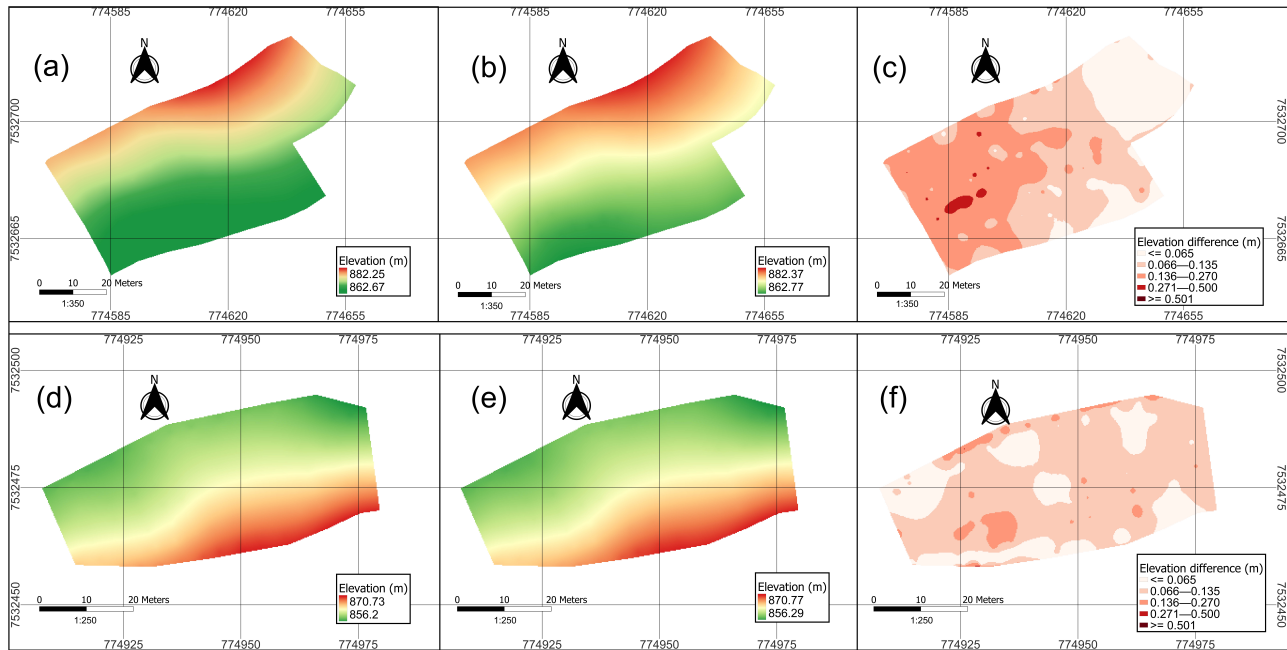


**Figure 12.** DEMs for areas 1 and 2 and the differences of DEM from both methodologies: (a) DEM of area 1, obtained by conventional topographic survey; (b) DEM of area 1, obtained using RPA; (c) altimetric difference between DEMs (a,b). (d) DEM of area 2, obtained by conventional topographic survey; (e) DEM of area 2, obtained using RPA; (f) altimetric difference between DEMs (d,e).

The maps represented in Figure 12c,f and Figure 13c,f show the differences among the DEMs for area 1, area 2, area 3, and area 4. Based on the area occupied by the classifications indicated on the maps ( $\leq 0.065$  m;  $0.066\text{--}0.135$  m;  $0.136\text{--}0.270$  m;  $0.271\text{--}0.500$  m;  $\geq 0.501$  m), the percentages of differences obtained in the total area measured (Table 1).

**Table 1.** Percentages of the differences among the DEMs in the total area.

Intervals of Difference among DEMs (m)	Area 1 (%)	Area 2 (%)	Area 3 (%)	Area 4 (%)
$\leq 0.065$	23.50	25.23	55.76	84.99
$0.066\text{--}0.135$	36.50	69.43	38.66	14.03
$0.136\text{--}0.270$	38.86	5.33	5.58	0.84
$0.271\text{--}0.500$	1.14	0.01	0.00	0.14
$\geq 0.501$	0.00	0.00	0.00	0.00

After generating the DEMs, slope maps were derived for all areas, repeating the map algebra operation (Figures 14 and 15).

The difference between the slope maps of area 1, area 2, area 3, and area 4 are represented sequentially by Figure 14c,f and Figure 15c,f. From the classifications presented in the maps ( $\leq 2.0\%$ ;  $2.1\text{--}4.0\%$ ;  $4.1\text{--}6.0\%$ ;  $\geq 6.1\%$ ), the percentage of occurrence of these intervals of differences in the total area was verified (Table 2).



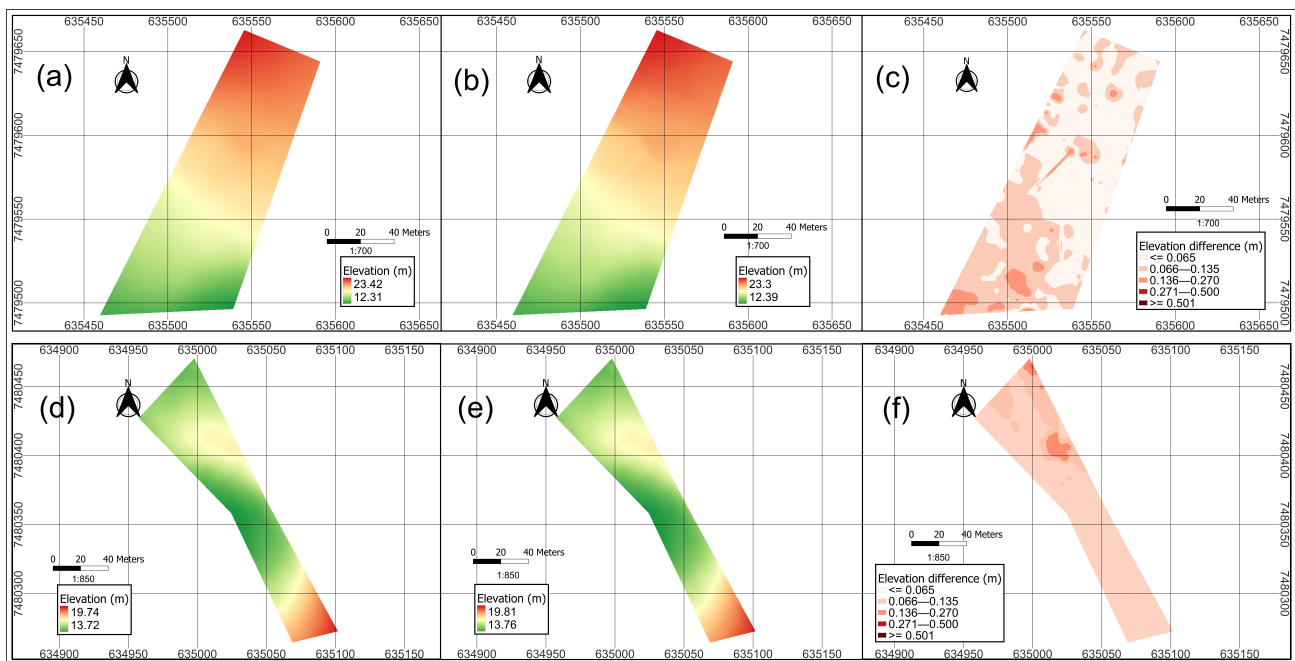


**Figure 13.** DEMs for areas 3 and 4 and the differences of DEM from both methodologies: (a) DEM of area 3, obtained by conventional topographic survey; (b) DEM of area 3, obtained using RPA; (c) altimetric difference between DEMs (a,b). (d) DEM of area 4, obtained by conventional topographic survey; (e) DEM of area 4, obtained using RPA; (f) altimetric difference between DEMs (d,e).

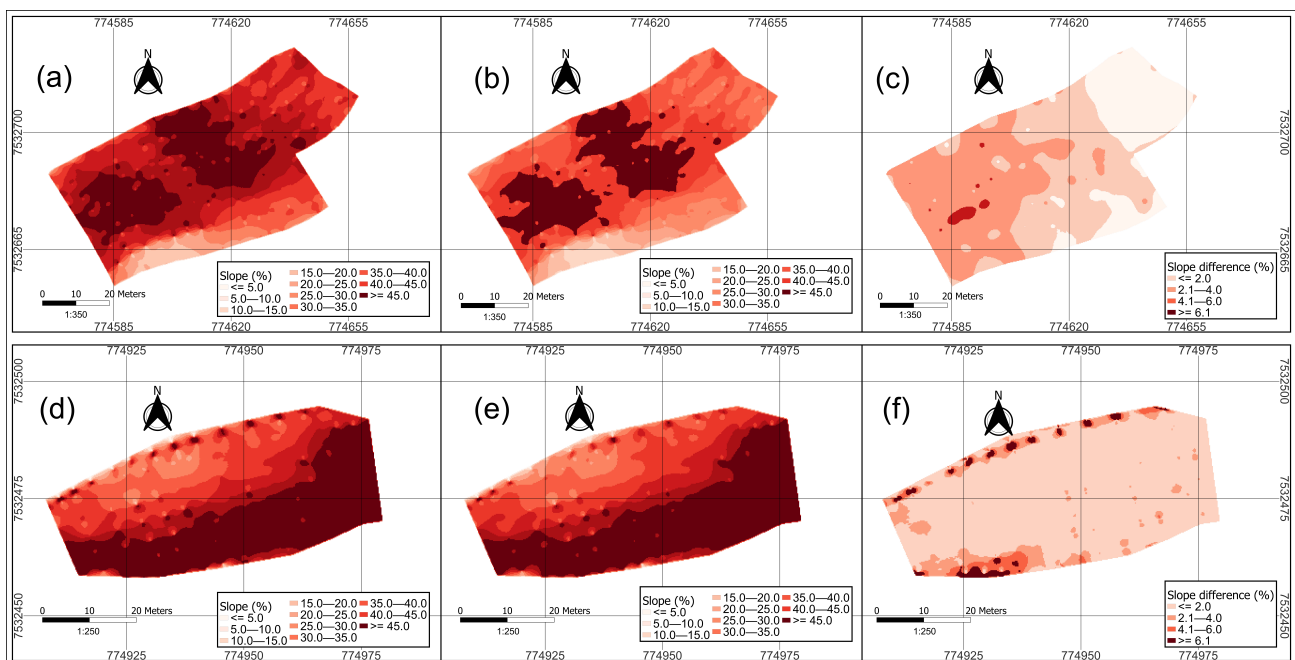


**Figure 14.** Slope maps for areas 1 and 2 and the differences in slope from both methodologies: (a) slope map of area 1, obtained by conventional topographic survey; (b) slope map of area 1 obtained using RPA; (c) difference between slope maps (a,b). (d) slope map of area 2 obtained by conventional topographic survey; (e) slope map of area 2 obtained using RPA; (f) difference between slope maps (d,e).



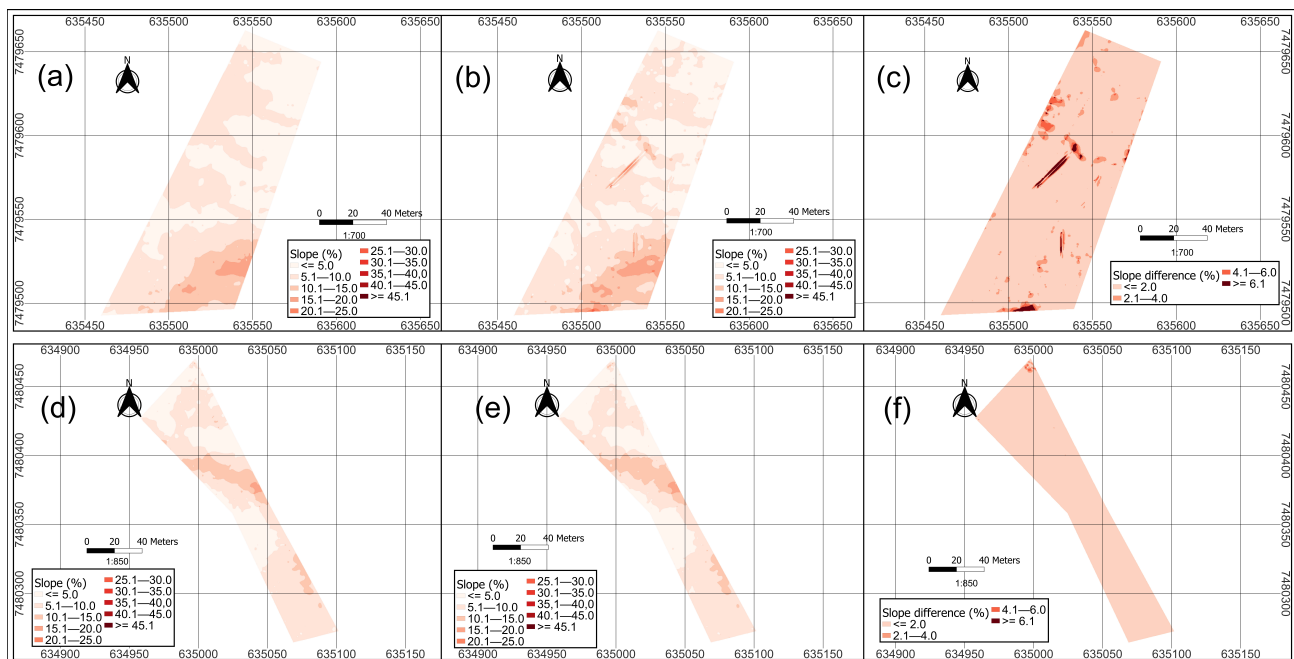


**Figure 15.** Slope maps for areas 3 and 4 and the differences in slope from both methodologies: (a) slope map of area 3, obtained by conventional topographic survey; (b) slope map of area 3, obtained using RPA; (c) difference in slope between maps (a,b). (d) slope map of area 4, obtained by conventional topographic survey; (e) slope map, of area 4, obtained using RPA; (f) difference in slope between maps (d,e).

**Table 2.** Occurrence percentages of the slope difference in the total area.

Slope Difference Intervals (%)	Area 1 (%)	Area 2 (%)	Area 3 (%)	Area 4 (%)
≤2.0	93.15	84.69	92.73	99.59
2.1–4.0	6.25	9.78	4.92	0.31
4.1–6.0	0.51	3.29	1.39	0.10
6.1	0.09	2.24	0.96	0.00

#### 4.2. Validation and Accuracy Analysis

Validation was performed after extracting the planimetric and altimetric coordinates of the 20 checkpoints determined by the topography (reference). The points were compared to their respective counterparts extracted from orthophotomosaics (planimetry) and DEMs (altimetry), generated after digital image processing obtained through RPA (test). Tables 3 and 4 sequentially present the results of the statistical parameters of the planimetric validations of the orthophotomosaics and altimetric of the DEMs.

**Table 3.** Result of the statistical parameters of planimetric validations of orthophotomosaics.

Parameters	Area 1	Area 2	Area 3	Area 4
$\bar{x}$ (m)	0.032	0.043	0.029	0.018
$\sigma$ (m)	0.019	0.037	0.019	0.008
max. (m)	0.078	0.112	0.071	0.036
min. (m)	0.010	0.000	0.000	0.010
RMSE <sub>x</sub> (m)	0.027	0.035	0.029	0.014
RMSE <sub>y</sub> (m)	0.025	0.044	0.018	0.014
RMSE <sub>r</sub> (m)	0.037	0.057	0.035	0.020



**Table 4.** Result of statistical parameters of DEM altimetric validations.

Parameters	Area 1	Area 2	Area 3	Area 4
$\bar{x}$ (m)	0.046	−0.003	0.039	0.022
$\sigma$ (m)	0.056	0.065	0.048	0.033
max. (m)	0.210	0.140	0.150	0.090
min. (m)	−0.050	−0.100	−0.050	−0.040
RMSE <sub>z</sub> (m)	0.071	0.063	0.061	0.039

The highest RMSE<sub>r</sub> values occurred in areas 1 and 2, whose average slopes are higher than areas 3 and 4, as they are areas classified as very rugged relief (Table 3). Similarly to what was perceived in the determination of the planimetric statistical parameters of the orthophotomosaics (Table 3), the highest values of RMSE<sub>z</sub> occurred in areas 1 and 2, whose behavior was already expected because they are areas with greater slopes when compared with areas 3 and 4 (Table 4).

The horizontal and vertical absolute accuracy values were independently determined at the 95% confidence level for the four study areas (Table 5).

**Table 5.** Horizontal and vertical absolute accuracy of the areas.

Parameters	Area 1	Area 2	Area 3	Area 4
Horizontal accuracy (m)	0.064	0.099	0.061	0.035
Vertical accuracy (m)	0.139	0.123	0.120	0.076

The results found in Table 5 for horizontal accuracy indicate that the worst value occurred for area 2, in the order of 0.099 m, whose average relief slope is higher than the others. While the best value occurred for area 4, in the order of 0.035 m, whose average relief slope is the smallest among all areas.

For vertical accuracy, area 1 presented the worst value (0.139 m) when compared to the other areas and area 4 presented the best overall result, in the order of 0.076 m. However, it is noteworthy that all areas presented a vertical accuracy smaller than the size of a pixel of the DEMs (0.20 m). The results found in the analysis of DEM vertical accuracy for areas 1 and 2 (very rugged relief) were similar to those found by Pedreira et al. [42]. The authors used 20 checkpoints to determine accuracy and performed an aerophotogrammetric survey in a single study area, dividing it into relief classes according to the slope. The altimetric accuracy results found by the authors for the relief class which is comparable to areas 1 and 2 of this study, were in the order of 0.125 m. In our study area, 1 presented a lower vertical accuracy value (0.139 m), however, area 2 was slightly higher (0.123 m). They found a vertical accuracy in the order of 0.156 m for the relief class similar to areas 3 and 4 of this work (smooth relief). Areas 3 and 4 presented vertical accuracy in the order of 0.120 and 0.076 m, respectively, therefore both were higher than those found by the authors [42].

#### 4.3. Similarity of Hausdorff Distance

After validating the aerophotogrammetric DEMs, contour lines were derived for each area. Concomitantly, the contour lines were generated using the conventional topographic survey. The contour lines were superimposed and the similarity evaluator software returned with the dH for each pair of homologous contour lines in each area, as shown in Table 6.

The results show that the best fit represented by the dH in area 1, occurred in the contour line of 881 m of elevation, with the measure of similarity in the order of 0.295 m. While in the contour line at 863 m of elevation, the measure of similarity found was 1.275 m, which is considered the worst fit in this representation.

The best fit represented by the dH in area 2 was found in the contour line at 869 m of elevation, with the similarity measure in the order of 0.218 m. The worst fit occurred in the contour line at 857 m of elevation, with a similarity measure of 0.573 m.



**Table 6.** Determination of dH for contour lines in areas 1 to 4.

Contour Line Elevation (m)	Hausdorff Distance (m)		Contour Line Elevation (m)	Hausdorff Distance (m)	
	Area 1	Area 2		Area 3	Area 4
857	-	0.573	13	1.046	-
858	-	0.382	14	2.005	0.983
859	-	0.448	15	1.570	1.400
860	-	0.448	16	2.247	0.290
861	-	0.424	17	3.102	0.238
862	-	0.354	18	1.372	0.187
863	1.275	0.416	19	2.808	0.223
864	1.096	0.334	20	2.083	-
865	0.535	0.388	21	2.861	-
866	0.663	0.262	22	1.677	-
867	0.545	0.352	23	3.011	-
868	0.765	0.258	-	-	-
869	0.600	0.218	-	-	-
870	0.547	0.249	-	-	-
871	0.637	-	-	-	-
872	0.560	-	-	-	-
873	0.551	-	-	-	-
874	0.491	-	-	-	-
875	0.572	-	-	-	-
876	0.841	-	-	-	-
877	0.581	-	-	-	-
878	0.592	-	-	-	-
879	0.331	-	-	-	-
880	0.437	-	-	-	-
881	0.295	-	-	-	-

The best fit indicated by the dH for area 3 occurred in the contour line at 13 m of elevation, in the order of 1.046 m. The worst fit was identified in the contour line at 17 m of elevation, in the order of 3.102 m.

The best fit by the dH in area 4 was in the contour line at 18 m of elevation, in the order of 0.187 m. The worst adjustment was found in the contour line at 15 m of elevation, in the order of 1.400 m.

From the dH data set presented in Table 6, the statistical parameters (mean, standard deviation, maximum and minimum) of the data set that represent all the contour lines of the same area were determined, as shown in Table 7.

**Table 7.** Statistical parameters of the dH analysis of the set of contour lines.

Parameters	Area 1	Area 2	Area 3	Area 4
$\bar{x}$ (m)	0.627	0.365	2.162	0.554
$\sigma$ (m)	0.235	0.097	0.707	0.512
<i>max.</i> (m)	1.275	0.573	3.102	1.400
<i>min.</i> (m)	0.295	0.218	1.046	0.187

The highest value of the mean and standard deviation of contour lines using dH was credited to area 3 (smooth relief), indicating the worst similarity. Additionally, area 4 (smooth relief) also presented a dispersion of data associated with dH higher than areas 1 and 2, even reporting a maximum value above these areas.

The lowest value observed for the mean and standard deviation of the contour lines associated with dH occurred in area 2 (very rugged relief). Area 1 (very rugged relief), despite having an average associated with dH higher than area 4, has better similarity than area 4, it has a higher number of contour lines than those arranged in area 4.

However, the dH must be interpreted in association with the correlated effects of the differences found between the DEMs and their respective slopes that occurred between



the data acquisition techniques. Figures 16 and 17 present the sets of contour lines derived from the two techniques, superimposed respectively on maps that represent differences in elevation and slope for the areas.

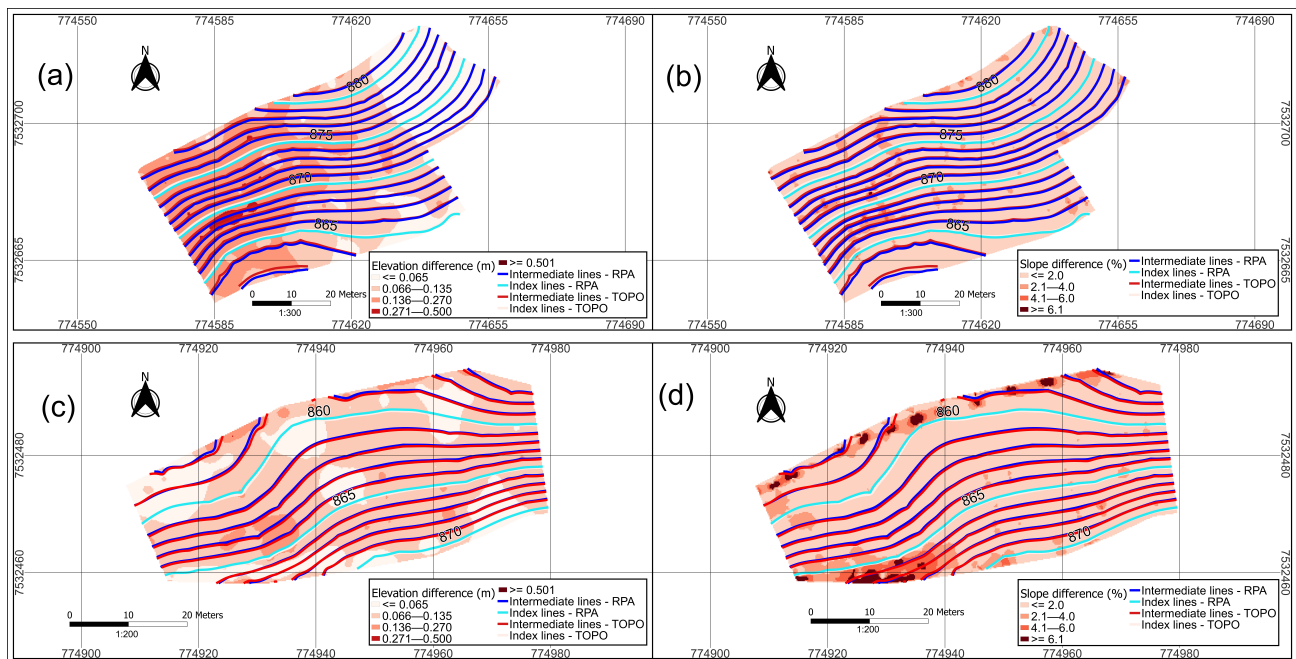


**Figure 16.** Superposition of homologous contour lines from topography and RPA of areas 1 and 2 over elevation and slope difference maps: (a) superposition of contour lines over DEM differences of area 1, (b) superposition of contour lines over slope differences of area 1, (c) superposition of contour lines over DEM differences of area 2, (d) superposition of contour lines over slope differences of area 2.

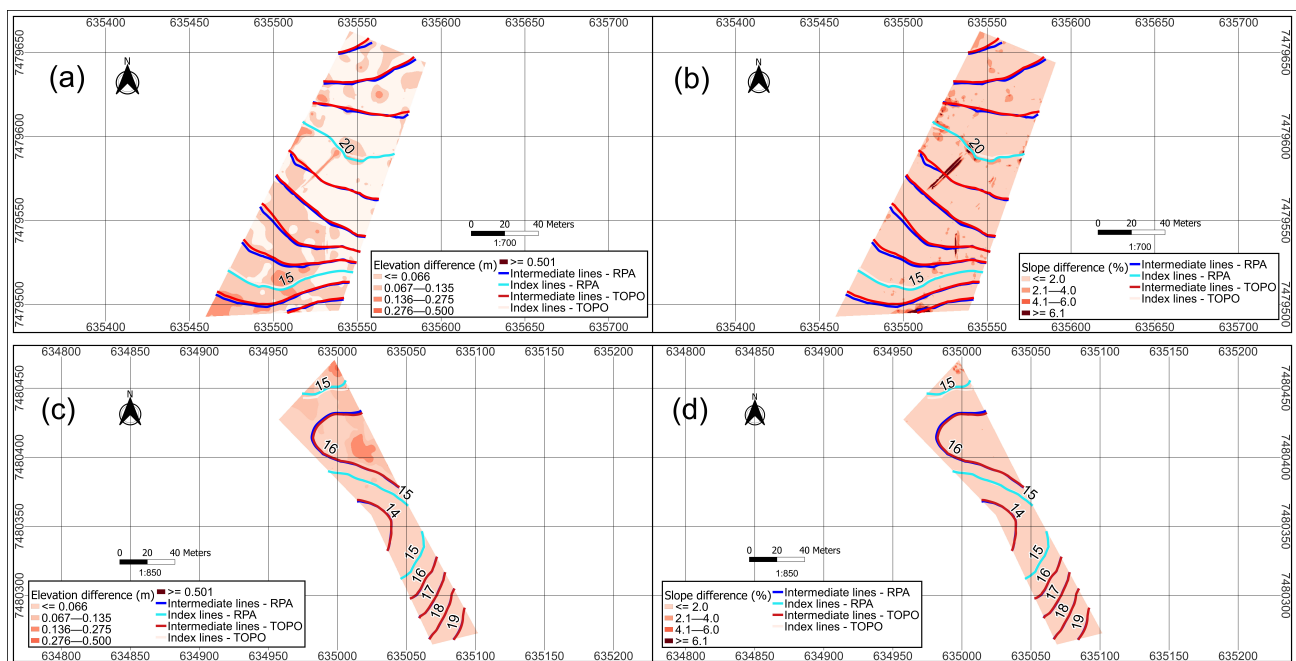


**Figure 17.** Superposition of homologous contour lines from topography and RPA of areas 3 and 4 over elevation and slope difference maps: (a) superposition of contour lines over DEM differences of area 3, (b) superposition of contour lines over slope differences of area 3, (c) superposition of contour lines over DEM differences of area 4, (d) superposition of contour lines over slope differences of area 4.



Considering the overlap in the differences of DEMs of the contour lines in area 1 (Figure 16a), we observed that the contour line at 881 m of elevation (best similarity) is inserted in a place with less altimetric divergence compared to the contour line at 863 m of elevation (worst similarity). However, the slope differences (Figure 16b) remain in a range of 0 to 2% where these curves are located.

In area 2, the contour line at the 869 m of elevation (best similarity) is located in lower altimetric divergences, when compared to the trajectory of the contour line at the elevation of 857 m (worst similarity), as shown in Figure 16c. In areas with these contour lines, the slope differences remained at 0 to 2% in almost the entire path of the contour lines, however presenting variations in small intervals of 2.1 to 4% for the contour line at the elevation of 869 m (Figure 16d). As for the contour line at the elevation of 857 m, the range from 0 to 2% of slope difference was predominant, but there were small stretches with values above 6.1% (Figure 16d).

In area 3 (Figure 17a), the contour lines at the elevation of 13 m (best similarity) and 17 m (worst similarity) were inserted in places with the same altimetric divergences. When checking the slope differences on these curves (Figure 17b), discrete stretches with variations in this parameter were observed. In the places where these curves are located, the slope differences remained in a range of 0 to 2% in most of their entire path, however, they present different intervals above 6.1% for both contour lines.

We found for area 4 (Figure 17c) that the contour lines at an elevation of 18 m (best similarity) passed through places with lower classes of altimetric differences when compared to the contour lines at an elevation of 15 m in the upper part of Figure 17c (worst similarity). No differences were observed in slope associated with dH in both curves (Figure 17d), as contour lines at 18 m and 15 m of elevation remained in a slope range difference from 0 to 2%.

The results found by the analysis of Hausdorff distance between homologous contour lines allows us to infer that this algorithm can be used to evaluate the accuracy of vector geometries. Gonçalves and Mitishita [43] also used Hausdorff distance for reviewing and updating urban maps by analyzing the similarity between vector geometries. After determining the quality and verifying the similarity of the features described by the contour lines obtained via RPA, a new perspective on using the RPAs for Precision Agriculture was introduced here. Martos et al. [44] describe the need to ensure sustainable agriculture, including the use of RPA technology to achieve this goal. Therefore, this work applies remote sensing with a robust methodology to achieve the goal described by Martos et al. [44], opening this segment to new perspectives of research and applications in Precision Agriculture.

## 5. Conclusions

In general, area 2 had the best similarity by the average of the data set provided by dH, while area 3 had the worst similarity. By comparing areas with similar reliefs, area 2 had smaller differences between the DEMs (topographic × RPA) and better vertical accuracy when compared to area 1. Both areas have a very rugged relief. This performance is repeated in the data found by similarity analysis when observing the general parameters of the dataset provided by dH. All indicators (average, standard deviation, maximum and minimum value) in area 2 were better than those found in area 1, according to Table 7.

For areas 3 and 4 classified as smooth relief, we found that area 4 presented the smallest differences between the DEMs (topographic × RPA), also associated with better vertical accuracy when compared to area 3. Area 3 and area 4 had the same performance when the similarity was evaluated by dH. All parameters evaluated (mean, standard deviation, maximum and minimum value) were better than those found in area 3, according to data in Table 7.

Although areas 3 and 4 have respectively presented the highest values associated with dH (3.102 m and 1.400 m), when compared to areas 1 and 2, whose maximum values were 1.275 m and 0.573 m, respectively, the differences between altimetry and slope were lower than those found in area 2 (best similarity of the set). The average slope rate of area 2 is



much higher than in areas 3 and 4. Therefore, the best general similarity found by applying the dH algorithm in area 2 did not mean a smaller difference between the DEMs, nor a better difference in slope when compared to areas with flatter reliefs.

The similarity by dH associated with vertical accuracy can be used as a quality indicator of an aerophotogrammetric product obtained by RPA when compared to the same product obtained by a source of superior precision. Therefore, the similarity algorithm used concomitantly with vertical accuracy is likely to be used for decision-making on issues involving application in precision agriculture.

Based on the results, the application of RPAs for the generation of contour lines proved to be a sufficiently effective technology capable of providing adequate contour planting. This finding is especially valid when analyzing the quantitative differences in slope, with the similarity obtained by the dH. It was noticed that the similarity obtained between the curves generated by topography and by RPA did not cause differences in slope greater than 6% in at least 95% of all study areas. This result indicates a high possibility of applying the contour lines derived from the RPA technology, for the safe application of contour planting.

In conclusion, the dH similarity algorithm can analyze the feasibility of contour planting with the products obtained by RPA according to the situations addressed in this study. The determination of vertical accuracy of Digital Elevation Models is of paramount importance and the Hausdorff similarity algorithm is a predictor of this quality by comparing different data acquisition techniques. Therefore, RPAs can generate contour lines for contour planting in Precision Agriculture, provided that vertical accuracy analysis controls the quality of the Digital Elevation Models.

**Author Contributions:** Conceptualization, A.A.R.F., M.A.H.A. and M.M.d.B.; methodology, A.A.R.F., M.A.H.A., M.M.d.B. and W.D.d.S.; software, W.D.d.S. and A.A.R.F.; validation, A.A.R.F., W.D.d.S. and T.M.d.S.; formal analysis, A.A.R.F. and M.A.H.A.; investigation, A.A.R.F. and T.M.d.S.; data curation, A.A.R.F. and W.D.d.S.; writing—original draft preparation, A.A.R.F. and T.M.d.S.; writing—review and editing, M.A.H.A., M.M.d.B. and W.D.d.S.; visualization, A.A.R.F., T.M.d.S., W.D.d.S. and W.D.d.S.; supervision, M.A.H.A. and M.M.d.B.; project administrator, A.A.R.F. All authors have read and agreed to the published version of the manuscript.

**Funding:** This research was financed by the Higher Education Personnel Improvement Coordination (CAPES) and by the Technical School of the Rural University (CTUR), both linked to the Federal Rural University of Rio de Janeiro (UFRRJ).

**Data Availability Statement:** Not applicable.

**Acknowledgments:** We thank the Coordination for the Improvement of Higher Education Personnel (CAPES), Technical School of the Rural University (CTUR), Federal Rural University of Rio de Janeiro (UFRRJ), and the Graduate Program in Science, Technology, and Innovation in Agriculture (PPGCTIA).

**Conflicts of Interest:** The authors declare no conflict of interest.

## References

1. Silva, L.L.; Baptista, F.; Cruz, V.F.; da Silva, J.R.M. Aumentar as competências dos agricultores para a prática de uma agricultura sustentável. *Rev. Ciências Agrárias* **2020**, *43*, 240–252. [\[CrossRef\]](#)
2. Neumann, P.S.; Loch, C. Legislação ambiental, desenvolvimento rural e práticas agrícolas. *Ciência Rural* **2002**, *32*, 243–249. [\[CrossRef\]](#)
3. Santos, F.S.; Amaral Sobrinho, N.M.B.; Mazur, N. Influência de diferentes manejos agrícolas na distribuição de metais pesados no solo e em plantas de tomate. *Rev. Bras. Ciência Solo* **2002**, *26*, 535–543. [\[CrossRef\]](#)
4. Griebeler, N.P.; Pruski, F.F.; Teixeira, A.F.; de Oliveira, L.F. Software to planning the use of level terracing systems in more rational ways. *Eng. Agrícola* **2005**, *25*, 841–851. [\[CrossRef\]](#)
5. Leite, E.F.; Rosa, R. Análise do uso, ocupação e cobertura da terra na bacia hidrográfica do Rio Formiga, Tocantins. *Rev. Eletrônica Geogr.* **2012**, *4*, 90–106.
6. Xavier, M.V.B.; Santos, L.L.; Fonseca, A.P.M.; de Almeida, E.S.; Almeida, L.V.O.; Aguiar, R.M.A.S.; Moreira, C.D.D.; Semensato, B.D.; Ferreira, J.M.; de Oliveira, P.V.A. Capacidade de uso e manejo conservacionista do solo de um fragmento de cerrado. *Res. Soc. Dev.* **2021**, *10*, e41410716697. [\[CrossRef\]](#)
7. Fortini, R.M.; Braga, M.J.; Freitas, C.O. Impacto das práticas agrícolas conservacionistas na produtividade da terra e no lucro dos estabelecimentos agropecuários brasileiros. *Rev. Econ. Sociol. Rural* **2020**, *58*, e199479. [\[CrossRef\]](#)



8. Paccioretti, P.; Córdoba, M.; Balzarini, M. FastMapping: Software to create field maps and identify management zones in precision agriculture. *Comput. Electron. Agric.* **2020**, *175*, 105–556. [\[CrossRef\]](#)
9. Yost, M.A.; Kitchen, N.R.; Sudduth, K.A.; Massey, R.E.; Sadler, E.J.; Drummond, S.T.; Volkmann, M.R. A long-term precision agriculture system sustains grain profitability. *Precis. Agric.* **2019**, *20*, 1177–1198. [\[CrossRef\]](#)
10. Nascimento, H.R.; de Abreu, Y.V. Geração de informações sobre a agricultura de energia por meio das geotecnologias. *Interações* **2012**, *13*, 181–189. [\[CrossRef\]](#)
11. Francisco, H.R.; Corrêia, A.F.; Feiden, A. Classification of areas suitable for fish farming using geotechnology and multi-criteria analysis. *ISPRS Int. J. Geo-Inf.* **2019**, *8*, 394. [\[CrossRef\]](#)
12. Hunt Jr, E.R.; Daughtry, C.S.T. What Good Are Unmanned Aircraft Systems for Agricultural Remote Sensing and Precision Agriculture. *Int. J. Remote Sens.* **2018**, *39*, 5345–5376. [\[CrossRef\]](#)
13. Maes, W.H.; Steppe, K. Perspectives for remote sensing with unmanned aerial vehicles in precision agriculture. *Trends Plant Sci.* **2019**, *24*, 152–164. [\[CrossRef\]](#) [\[PubMed\]](#)
14. Bendig, J.; Yu, K.; Aasen, H.; Bolten, A.; Bennertz, S.; Broscheit, J.; Gnyp, M.L.; Bareth, G. Combining UAV-Based plant height from crop surface models, visible, and near-infrared vegetation indices for biomass monitoring in barley. *Int. J. Appl. Earth Obs. Geoinf.* **2015**, *39*, 79–87. [\[CrossRef\]](#)
15. Pérez-Ortiz, M.; Peña, J.M.; Gutiérrez, P.A.; Torres-Sánchez, J.; Hervás-Martínez, C.; López-Granados, F. Selecting patterns and features for between- and within- crop-row weed mapping using UAV-imagery. *Expert Syst. Appl.* **2016**, *47*, 85–94. [\[CrossRef\]](#)
16. Chang, A.; Jung, J.; Maeda, M.M.; Landivar, J. Crop height monitoring with digital imagery from Unmanned Aerial System (UAS). *Comput. Electron. Agric.* **2017**, *141*, 232–237. [\[CrossRef\]](#)
17. Schut, A.G.T.; Traore, P.C.S.; Blaes, X.; By, R.A. Assessing yield and fertilizer response in heterogeneous smallholder fields with UAVs and satellites. *Field Crops Res.* **2018**, *221*, 98–107. [\[CrossRef\]](#)
18. Tsouros, D.C.; Bibi, S.; Sarigiannidis, P.G. A review on UAV-based applications for precision agriculture. *Information* **2019**, *10*, 349. [\[CrossRef\]](#)
19. Santos, L.M.; Ferraz, G.A.S.; Barbosa, B.D.S.; Andrade, A.D. Use of remotely piloted aircraft in precision agriculture: A review. *Dyna* **2019**, *86*, 284–291. [\[CrossRef\]](#)
20. Delavarpour, N.; Koparan, C.; Nowatzki, J.; Bajwa, S.; Sun, X. A technical study on UAV characteristics for precision agriculture applications and associated practical challenges. *Remote Sens.* **2021**, *13*, 1204. [\[CrossRef\]](#)
21. Nemmaoui, A.; Aguilar, F.J.; Aguilar, M.A.; Qin, R. DSM and DTM generation from VHR satellite stereo imagery over plastic covered greenhouse areas. *Comput. Electron. Agric.* **2019**, *164*, 104903. [\[CrossRef\]](#)
22. Akturk, E.; Altunel, A.O. Accuracy assessment of a low-cost UAV derived digital elevation model (DEM) in a highly broken and vegetated terrain. *Meas. J. Int. Meas. Confed.* **2019**, *136*, 382–386. [\[CrossRef\]](#)
23. Mukherjee, A.; Misra, S.; Raghuvanshi, N.S. A survey of unmanned aerial sensing solutions in precision agriculture. *J. Netw. Comput. Appl.* **2019**, *148*, 102461. [\[CrossRef\]](#)
24. Iticha, B.; Takele, C. Digital soil mapping for site-specific management of soils. *Geoderma* **2019**, *351*, 85–91. [\[CrossRef\]](#)
25. Santana, L.S.; Ferraz, G.A.e.S.; Marin, D.B.; Faria, R.d.O.; Santana, M.S.; Rossi, G.; Palchetti, E. Digital Terrain Modelling by Remotely Piloted Aircraft: Optimization and Geometric Uncertainties in Precision Coffee Growing Projects. *Remote Sens.* **2022**, *14*, 911. [\[CrossRef\]](#)
26. Marchi, E.C.S.; Campos, K.P.; Corrêa, J.B.D.; Guimarães, R.J.; Souza, C.A.S. Sobrevivência de mudas de cafeeiro produzidas em sacos plásticos e tubetes no sistema convencional e plantio direto, em duas classes de solo. *Ceres* **2003**, *50*, 407–416.
27. Solos, E. *Sistema Brasileiro de Classificação de Solos*, 2nd ed.; Centro Nacional de Pesquisa de Solos: Rio de Janeiro, Brazil, 2006; p. 306.
28. Esri, R. *ArcGIS Desktop*; Environmental Systems Research Institute: Redlands, CA, USA, 2016.
29. Hutchinson, M.F. A new procedure for gridding elevation and stream line data with automatic removal of spurious pits. *J. Hydrol.* **1989**, *106*, 211–232. [\[CrossRef\]](#)
30. Oikonomou, C.; Stathopoulou, E.K.; Georgopoulos, A. Contemporary data acquisition technologies for large scale mapping. In Proceedings of the 35th EARSeL Symposium—European Remote Sensing: Progress, Challenges and Opportunities, Stockholm, Sweden, 15–18 June 2015.
31. Westoby, M.J.; Brasington, J.; Glasser, N.F.; Hambrey, M.J.; Reynolds, J.M. ‘Structure-from-Motion’ photogrammetry: A low-cost, effective tool for geoscience applications. *Geomorphology* **2012**, *179*, 300–314. [\[CrossRef\]](#)
32. Zanetti, J.; Braga, F.L.S.; Dos Santos, A.d.P. Comparativo das normas de controle de qualidade posicional de produtos cartográficos do Brasil, da ASPRS e da OTAN. *Rev. Bras. Cartogr.* **2018**, *70*, 359–390. [\[CrossRef\]](#)
33. Mora, O.E.; Chen, J.; Stoiber, P.; Koppányi, Z.; Pluta, D.; Josenhans, R.; Okubo, M. Accuracy of stockpile estimates using low-costsUAS photogrammetry. *Int. J. Remote Sens.* **2020**, *41*, 4512–4529. [\[CrossRef\]](#)
34. American Society for Photogrammetry and Remote Sensing (ASPRS). ASPRS Positional Accuracy Standards for Digital Geospatial Data. *Photogramm. Eng. Remote Sens.* **2015**, *81*, A1–A26.
35. Ghilani, C.D.; Wolf, P.R. *Adjustment Computations: Spatial Data Analysis*, 4th ed.; John Wiley & Sons, Inc.: Hoboken, NJ, USA, 2006; pp. 326–327. [\[CrossRef\]](#)
36. López, F.J.A. Calidad en la producción cartográfica. *Mapping* **2003**, *84*, 96–98.
37. Gregoire, N.; Bouillot, M. Hausdorff Distance between convex polygons. *Comput. Geom. Web Proj.* **1998**, *8*, 2008.



38. Santos, A.D.P.D.; Medeiros, N.D.G.; Santos, G.R.D.; Rodrigues, D.D. Controle de qualidade posicional em dados espaciais utilizando feições lineares. *Bol. De Ciências Geodésicas*. **2015**, *21*, 233–250. [[CrossRef](#)]
39. Elmasri, R.; Navathe, S.B. *Fundamentals of Database Systems*, 7th ed.; University of Texas at Arlington Georgia Institute of Technology: Arlington, TX, USA, 2016; p. 1280.
40. Butler, H.; Daly, M.; Doyle, A.; Gillies, S.; Hagen, S.; Schaub, T. The geojson format. *Internet Eng. Task Force (IETF)* **2016**, RFC 7946, 1–28.
41. Butler, H.; Daly, M.; Doyle, A.; Gillies, S.; Schaub, T.; Schmidt, C. GeoJSON. Electronic. 2014. Available online: <http://geojson.org> (accessed on 26 May 2022).
42. Pedreira, W.J.P.; de Andrade Oliveira, J.; Santos, P.S. Avaliação da Acurácia Altimétrica usando a Tecnologia VANT. *Rev. Caminhos Geogr.* **2020**, *21*, 209–222. [[CrossRef](#)]
43. Gonçalves, G.A.; Mitishita, E.A. O Uso da Distância de Hausdorff como Medida de Similaridade em Sistemas Automáticos de Atualização Cartográfica. *Bol. Ciências Geodésicas*. **2016**, *22*, 719–735. [[CrossRef](#)]
44. Martos, V.; Ahmad, A.; Cartujo, P.; Ordoñez, J. Ensuring agricultural sustainability through remote sensing in the era of agriculture 5.0. *Appl. Sci.* **2021**, *11*, 5911. [[CrossRef](#)]